J. Fluid Mech. (1980), *vol.* 100, *part* 4, *pp.* 769–783
Printed in Great Britain

Free convection from a heated sphere at large Grashof number

By JANET M. POTTER AND N. RILEY

School of Mathematics and Physics,
University of East Anglia, Norwich

(Received 23 May 1979 and in revised form 22 February 1980)

We consider the free-convective flow from a heated sphere, in the Boussinesq approximation, at high Grashof number. The characteristics of the boundary layer close to the surface of the sphere are evaluated numerically, and the eruption of the fluid from the boundary layer into the plume above the sphere is discussed.

1. Introduction

When a heated body is placed in a fluid which is otherwise at rest density differences within the fluid result in an upward convective motion. Ultimately, as long as the flow remains steady, the rising fluid will assume the classical plume form discussed briefly by Prandtl (1952). The plume is characterized by the heat flux along it due to the transfer of heat from the body, which acts effectively as a point source of heat. In this paper we consider the convective flow which arises when a heated sphere is placed in a fluid which is otherwise at rest. We consider the flow for large values of a suitably defined Grashof number. The Boussinesq approximation is employed throughout.

In § 2 we present numerical solutions for the boundary layer which forms at the surface of the heated sphere at large Grashof number. We compare our results with earlier approximate and large-Prandtl-number asymptotic theories (Merk & Prins 1954; Chiang, Ossin & Tien 1964; Acrivos 1960), and with the experiments, carried out in air, by Bromham & Mayhew (1962). We find that first-order boundary-layer theory underestimates the overall heat transfer from the sphere, and that the discrepancy between theory and experiment may be attributed to finite-Grashof-number effects. From our numerical solution we note in particular that as the moving fluid converges onto the upper stagnation point the solution exhibits a singular behaviour, and the boundary layer erupts into the plume which forms above the sphere. The scale of the eruption region, within which the flow is governed by the inviscid Euler equations, is predicted from the nature of the singularity, and it is shown that this region is much thicker than the boundary layer which forms over the sphere surface. Experimental evidence in favour of this prediction is provided by the work of Kranse & Schenk (1965), Amato & Tien (1972) and Jaluria & Gebhart (1975).

The fluid emerges from the eruption region to form the plume, which we discuss in § 3. Initially, in the plume, viscous and diffusive effects are unimportant, the fluid accelerates as a body falling freely under gravity and the diameter of the plume steadily decreases. Measurements by Jaluria & Gebhart (1975), of the centre-line velocity and temperature, in this part of the plume region, tend to support our

0022-1120/80/4646-2340 $02.00

theoretical description of the flow. Ultimately viscous effects are non-negligible, and the classical plume solution is finally recovered at a large distance above the sphere, whose effect is then that of a point source of heat.

2. Boundary layer on the sphere

The equations which govern a buoyancy-driven, steady laminar motion in the Boussinesq approximation, that is where variable fluid properties are ignored except in the buoyancy term, are

$$\left.\begin{aligned} (\mathbf{v}.\nabla)\,\mathbf{v} &= -\frac{1}{\rho_\infty}\nabla p + \nu_\infty \nabla^2 \mathbf{v} - \frac{\rho-\rho_\infty}{\rho_\infty}\mathbf{g}, \\ \nabla.\mathbf{v} &= 0, \\ (\mathbf{v}.\nabla)\,T &= \kappa_\infty \nabla^2 T. \end{aligned}\right\} \tag{1}$$

In these equations $\mathbf{v}$ is the velocity vector, p the pressure, T the temperature, ρ the density, ν the kinematic viscosity, κ the thermal diffusivity, and $\mathbf{g}$ the acceleration due to gravity. A subscript ∞ denotes the conditions in some ambient or reference state.

Our concern is with the flow about a heated sphere, radius a, whose surface is maintained at a uniform temperature T_w. The equations (1) are made dimensionless with a as a typical length and $\{ga(T_w-T_\infty)/T_\infty\}^{\frac{1}{2}}$ a typical velocity. A dimensionless temperature θ is defined as $\theta = (T-T_\infty)/(T_w-T_\infty)$. In a boundary-layer flow, as in region I of figure 1, the pressure is uniform across the boundary layer. Thus, if the pressure is uniform outside the boundary layer, as it is to leading order in the asymptotic solution for the high-Grashof-number flows under consideration, then it is uniform everywhere and the equation of state reduces to

$$\rho T = \rho_\infty T_\infty. \tag{2}$$

We now introduce, with reference to figure 1, boundary-layer co-ordinates (x, Y) as

$$x = \pi - \phi, \quad \epsilon^{\frac{1}{2}} a Y = r - a, \tag{3}$$

with corresponding velocity components $u(x, Y), \epsilon^{\frac{1}{2}} V(x, Y)$. Here the small parameter ϵ is related to the Grashof number Gr by

$$\epsilon^2 = Gr^{-1} = \frac{\nu_\infty^2 T_\infty}{ga^3(T_w-T_\infty)}. \tag{4}$$

In terms of the co-ordinates (x, Y), and in the limit $\epsilon \to 0$, the dimensionless equations for continuity, momentum and energy are, from (1), (2) and (3),

$$\frac{\partial}{\partial x}(u \sin x) + \frac{\partial}{\partial Y}(V \sin x) = 0, \tag{5a}$$

$$u\frac{\partial u}{\partial x} + V\frac{\partial u}{\partial Y} = \frac{\partial^2 u}{\partial Y^2} + \theta \sin x, \tag{5b}$$

$$u\frac{\partial \theta}{\partial x} + V\frac{\partial \theta}{\partial Y} = \frac{1}{\sigma}\frac{\partial^2 \theta}{\partial Y^2}, \tag{5c}$$

where $\sigma = \nu_\infty/\kappa_\infty$ is the Prandtl number. The boundary conditions for equations (5) are

$$\left.\begin{aligned} &u = V = 0, \quad \theta = 1 \quad \text{at} \quad Y = 0, \\ &u, \theta \to 0 \quad \text{as} \quad Y \to \infty. \end{aligned}\right\} \tag{6}$$

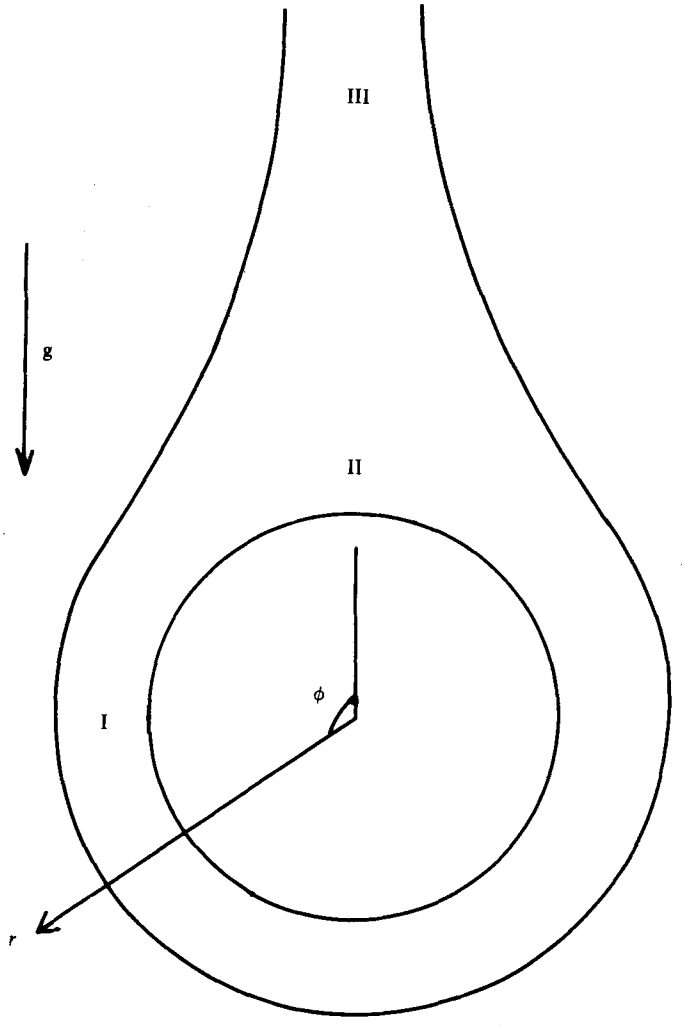

FIGURE 1. Schematic representation of the flow. I, the sphere boundary layer; II, the eruption region; III, the plume.

Equations (5) and (6), which do not admit a solution of self-similar form, together with their two-dimensional analogues have been studied by Merk & Prins (1954) by approximate methods. Thus with assumed forms for the velocity and temperature profiles a momentum integral approximation is used and the resulting forms of (5) are expanded in series in powers of x up to $O(x^{12})$. Merk & Prins also take advantage of the simplifying features associated with case $\sigma \gg 1$ in their approximate scheme. Similarly Acrivos (1960), who is concerned with free convection in non-Newtonian fluids for a variety of two- and three-dimensional configurations, takes advantage of the large-Prandtl-number simplifications in (5) and derives an exact form for the leading term in the asymptotic expansion of the solution as $\sigma \to \infty$. For arbitrary values of σ Chiang *et al.* (1964) propose a series solution of (5) in powers of x with coefficients that satisfy ordinary differential equations. In the examples given only the first two terms of the series are evaluated. Watson & Poots (1972) consider a

more complicated set of equations than (5) to study the free-convective flow over a heated ellipsoid of which the sphere is a special case. Their method is a hybrid method in which a series solution in one surface co-ordinate is adopted, whilst finite-difference methods are used to solve the partial differential equations in the other surface co-ordinate, corresponding to our variable x, and the co-ordinate measured normal to the wall. Their calculations terminate at $x = 2{\cdot}5$.

Close to $x = 0$ the solution of (5) is of the type which is familiar at a point of attachment, and which forms the leading term in the series of Chiang *et al.*, namely

$$u = xf_0'(Y), \quad V = -2f_0(Y), \quad \theta = \theta_0(Y),$$

where f_0, θ_0 satisfy the ordinary differential equations

$$\left.\begin{aligned} f_0''' + 2f_0 f_0'' - f_0'^2 + \theta_0 &= 0, \\ \theta_0'' + 2\sigma f_0 \theta_0' &= 0, \\ f_0(0) = f_0'(0) = 0, \quad \theta_0(0) &= 1, \\ f_0', \theta_0 \to 0 \quad \text{as} \quad Y &\to \infty. \end{aligned}\right\} \tag{7}$$

with

The numerical solution of these equations provides us with conditions, for the set of equations (5), at $x = 0$.

With initial conditions from (7), equations (5) have been integrated numerically, with $\sigma = 0{\cdot}72$, subject to (6). Thus in advancing the solution from $x = x_1$ to $x = x_2$ derivatives with respect to x are represented by central differences, and other quantities are averaged between the two stations; derivatives with respect to Y are also represented by central differences. Since the equations are nonlinear an iterative scheme has been employed within which we write

$$u\frac{\partial u}{\partial x} \approx \tilde{u}\frac{\partial u}{\partial x} + u\frac{\partial \tilde{u}}{\partial x} - \tilde{u}\frac{\partial \tilde{u}}{\partial x},$$

where if u is the current value of the velocity a tilde denotes its value at the previous iteration. The iterative procedure at a given station commences by estimating u at that station by a suitable extrapolation from values at earlier stations. The velocity component V is then calculated from (5a) and the temperature θ from (5c). An updated estimate of u is then obtained from (5b). This cycle of operations is repeated until the difference in the calculated values of the flow variables between successive iterates falls below some prescribed value, at which point the iterative scheme is deemed to have converged and the whole process advances to the next station. A step length $\delta Y = 0{\cdot}1$ in the Y direction was used in the calculations, with $\delta x = 0{\cdot}1$ up to the point at which x derivatives became large. Thus for $x > 2{\cdot}7$ a value $\delta x = 0{\cdot}01$ was used. The maximum value of Y, at which the outer conditions were applied, was adjusted to accommodate the thickening boundary layer up to $Y = 100$. We were thus able to obtain satisfactory results up to $x = 3{\cdot}02$, at which point the structure of the solution as $x - \pi \to 0$ had clearly emerged. At the suggestion of a referee we repeated the calculations with step lengths $2\delta x$ and $2\delta Y$ in order to check the trends observed in our results. In particular from each of our fine and coarse mesh solutions we have extrapolated the wall values of shear stress $\partial u/\partial Y$ and heat transfer $\partial\theta/\partial Y$ to zero. From the results obtained we have employed h^2-extrapolation to determine in each case the value $x = 3{\cdot}141$ at which these quantities vanish. We interpret this

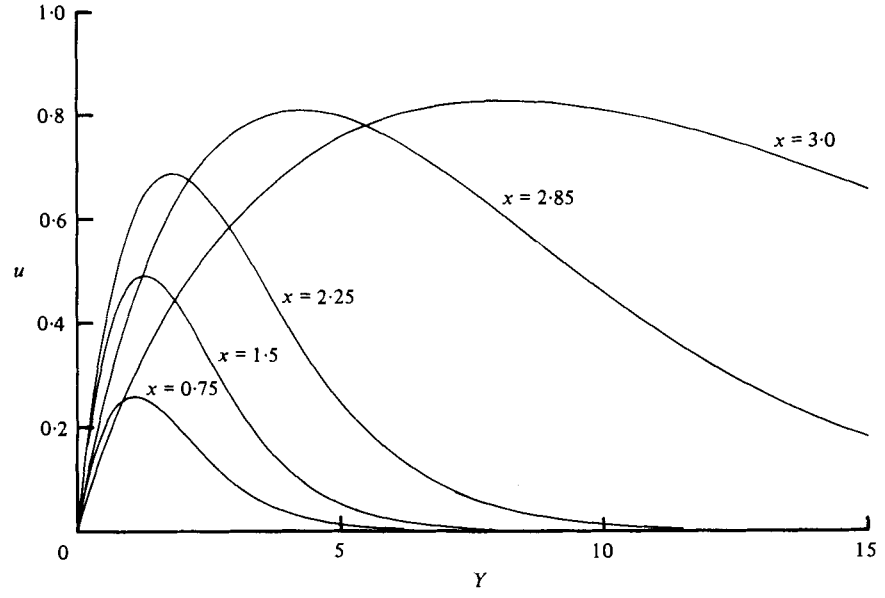

FIGURE 2. Velocity profiles, at various stations, in the boundary layer on the sphere for $\sigma = 0{\cdot}72$.

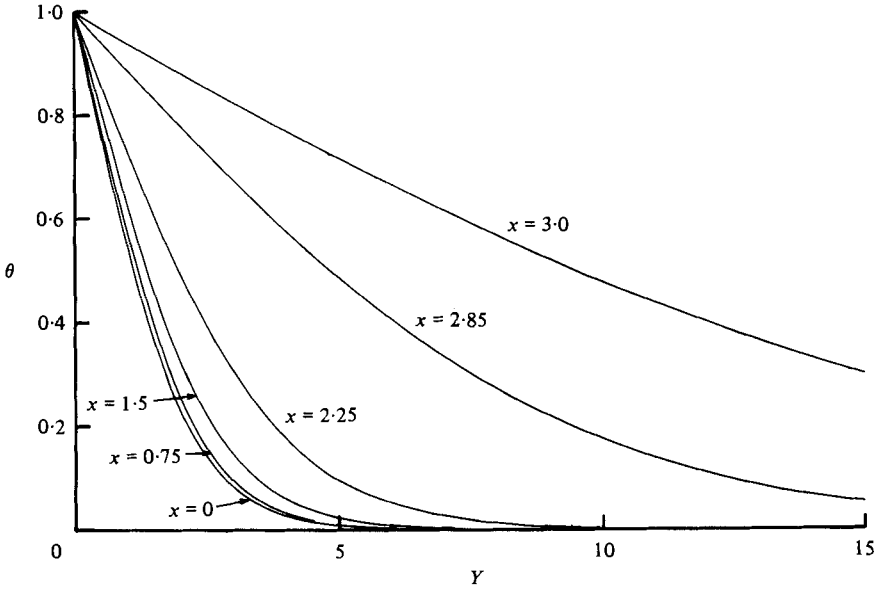

FIGURE 3. Temperature profiles, at various stations, in the boundary layer on the sphere for $\sigma = 0{\cdot}72$.

result as $x = \pi$ within our numerical approximation. This suggests that flow separation does not occur for $x < \pi$. We discuss the problem of flow separation from the sphere, or eruption into the plume which forms above it, in more detail below, where we also consider the singular behaviour exhibited by our results as $x \to \pi$.

Velocity and temperature profiles for various values of x are shown in figures 2 and 3. A feature of the results shown, as evidenced by the amount of fluid which is

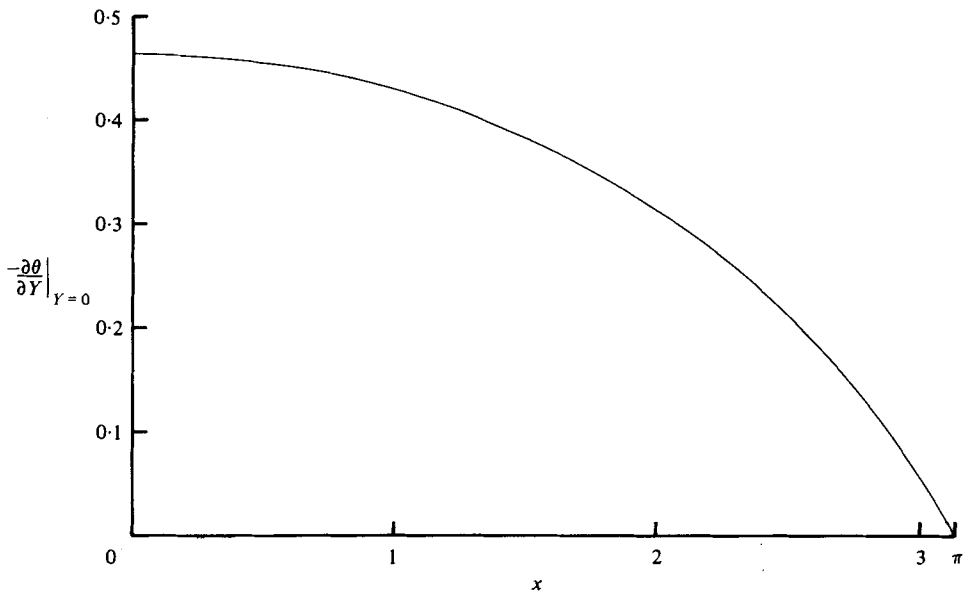

FIGURE 4. The local heat transfer rate $-\partial\theta/\partial Y|_{Y=0}$ over the surface of the sphere for $\sigma = 0{\cdot}72$.

heated and consequently set into motion, is that although the fluid velocity increases continuously under the action of buoyancy forces the boundary-layer thickness remains almost constant up to $x = \frac{1}{2}\pi$. Thereafter a thickening of the boundary layer is evident, with the maximum velocity tending to a constant. A closer examination of the numerical results suggests that the maximum velocity indeed remains finite (which is to be expected as the driving force decreases) whilst the boundary-layer thickness becomes unbounded in the limit $x \to \pi$. This latter result was conjectured by Merk & Prins (1954), and is discussed in more detail below. In figure 4 we show the local heat-transfer variation over the surface of the sphere. This distribution is qualitatively consistent with the high-Prandtl-number theory of Acrivos (1960), and is in reasonable quantitative agreement with the approximate theory of Merk & Prins (1954), which does however overestimate the heat transfer. The two-term series solution of Chiang *et al.* cannot adequately describe the flow over the whole of the sphere, and predicts a non-zero value at the upper stagnation point for the local heat transfer which is about one quarter of the value at the lower stagnation point.

The total heat transfer Q from the sphere is given by

$$Q = -2\pi a^2\lambda \int_0^\pi \frac{\partial T}{\partial r}\bigg|_{r=a} \sin\phi\, d\phi$$

$$= -2\pi a\lambda(T_w - T_\infty)\epsilon^{-\frac{1}{4}} \int_0^\pi \frac{\partial\theta}{\partial Y}\bigg|_{Y=0} \sin x\, dx, \tag{8}$$

where λ is the thermal conductivity of the fluid. From (8) and our numerical results, we have calculated the Nusselt number Nu as

$$Nu = \frac{Q}{\lambda a(T_w - T_\infty)} = 4{\cdot}395\epsilon^{-\frac{1}{4}}. \tag{9}$$

It is common in the literature to express the Nusselt number in the form $Nu = C(\sigma Gr)^{\frac{1}{4}}$ for $Gr \gg 1$ (see, for example, Merk & Prins 1954; Acrivos 1960). For our calculations, with $\sigma = 0{\cdot}72$, we have, from (9), $C = 4{\cdot}805$. For comparison, and with a correction made to accord with the notation of the present paper, the exact theory of Acrivos (1960) for $\sigma \gg 1$ gives $C = 5{\cdot}18$ whilst the approximate theory of Merk & Prins (1954) gives $C = 5{\cdot}01$ for $\sigma = 0{\cdot}7$ and $C = 5{\cdot}90$ for $\sigma \gg 1$, and the series of Chiang *et al.* with $\sigma = 0{\cdot}7$, $C = 4{\cdot}92$. With experiments in air, at a Prandtl number comparable to that which we have used, Bromham & Mayhew (1962) give $C = 5{\cdot}2$. With benzene as the working fluid, which with $\sigma = 8{\cdot}3$ may be considered to be a high-Prandtl-number fluid, Kranse & Schenk (1965) give $C = 6{\cdot}2$ whilst, for experiments in water, for which $\sigma = 7$, Amato & Tien (1972) give $C = 5{\cdot}3$. A deviation between results based on first-order boundary-layer theory and experiment is to be expected due to finite-Grashof-number effects. Thus the local heat transfer results of Kranse & Schenk (1965) show a monotonic decrease until $x \approx 2{\cdot}5$, after which the heat transfer rises until the upper stagnation point is reached. This departure from the theoretical first-order boundary-layer theory gives an indication of the extent of finite-Grashof-number effects in the neighbourhood of the upper stagnation point, and also shows that the measured heat transfer will be slightly in excess of that predicted by such a theory. We consider next the behaviour of our numerical solution in the neighbourhood of the upper stagnation point.

The rapid thickening of the boundary layer as $x \to \pi$, which we have already noted, is associated with an anticipation by the converging flow of the upper stagnation point. In this respect the flow differs from its two-dimensional analogue, and we consider this difference in more detail below. In the present calculations, for values of x up to $x \approx 1{\cdot}7$, $V < 0$ throughout the boundary layer as we might expect for an entraining flow. However in the central parts of the boundary layer not only does the sign of V eventually change but it also becomes increasingly large, and is $O(10^2)$ at $x = 3$. In these regions viscous forces are relatively unimportant when compared with inertia and buoyancy forces. Of course, as $Y \to \infty$, V again becomes negative and so assumes the values associated with viscous entrainment.

The structure of the singularity in the solution as $x \to \pi$, i.e. $\phi \to 0$, may be determined as follows. The numerical results suggest that, whereas the boundary-layer thickness and normal velocity V become unbounded in this limit, both u and θ remain finite. Thus, as $\phi \to 0$, we write

$$u = u_0(\eta), \quad \theta = \theta_0(\eta), \quad V = v_0(\eta)\,\Delta(\phi), \quad \eta = \frac{Y}{\delta(\phi)},$$

and substitution into (5*a*) and (5*b*) gives, to leading order,

$$\left.\begin{aligned} u_0 - \phi\,\frac{\dot{\delta}}{\delta}\,\eta u_0' - \frac{\phi\Delta}{\delta}\,v_0' = 0, \\ v_0 = -\eta u_0\,\frac{\dot{\delta}}{\Delta}, \end{aligned}\right\}$$

where a prime and a dot denote differentiation with respect to η and ϕ respectively. Elimination of v_0 between these equations gives

$$u_0\left(1 + \frac{\phi\dot{\delta}}{\delta}\right) = 0;$$

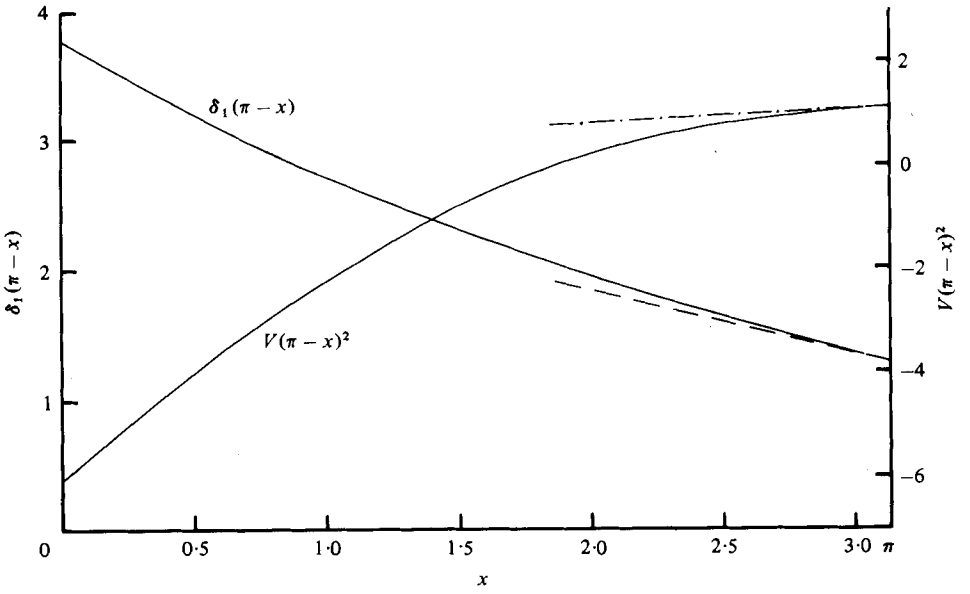

FIGURE 5. The variation of $V(\pi - x)^2$ and $\delta_1(\pi - x)$ at the location $\theta = \frac{1}{2}$ in the boundary layer, together with their asymptotic forms, deduced from the numerical solution $1{\cdot}089 - 0{\cdot}232(\pi - x)$ (–·–·–·–) and $1{\cdot}279 + 0{\cdot}496(\pi - x)$ (– – – – –) respectively.

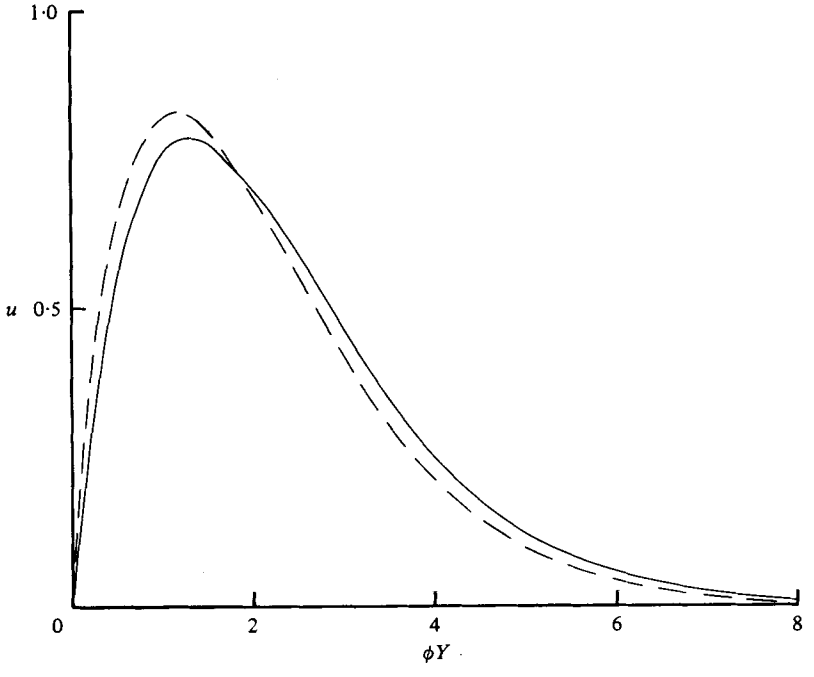

FIGURE 6. Velocity profiles close to the upper stagnation point as functions of $Z = \phi Y$ ($\phi = \pi - x$) for $\sigma = 0{\cdot}72$; ——, $\phi = 0{\cdot}442$; – – – –, $\phi = 0{\cdot}142$.

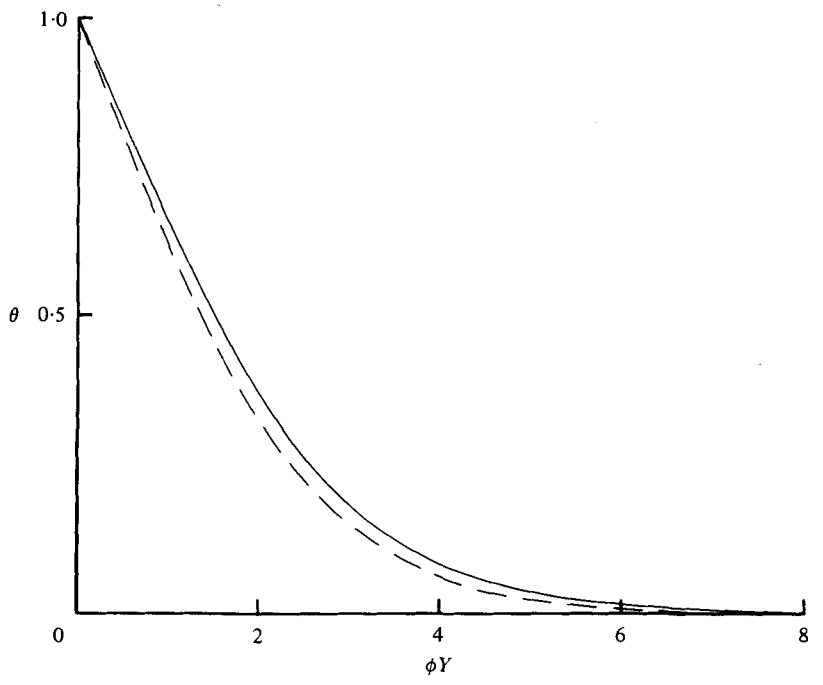

FIGURE 7. Temperature profiles close to the upper stagnation point as functions of $Z = \phi Y$ ($\phi = \pi - x$) for $\sigma = 0{\cdot}72$; ——, $\phi = 0{\cdot}442$; – – – –, $\phi = 0{\cdot}142$.

thus $\delta \propto \phi^{-1}$, and it then follows that $\Delta \propto \phi^{-2}$. These predictions are fully confirmed by our numerical results. Thus if $Y = \delta_1$ denotes the location at which $\theta = \frac{1}{2}$ we have examined $(\pi - x)\,\delta_1$ and $(\pi - x)^2\,V$ at $Y = \delta_1$ and shown that they are finite as $x \to \pi$. These quantities are shown in figure 5 together with their limiting values deduced from the numerical results. In figures 6 and 7 we show velocity and temperature profiles from our numerical solution plotted as functions of ϕY, for different values of $\phi = \pi - x$, which show how limiting values are approached, and further confirms the singular nature of the solution, discussed above, as $x \to \pi$.

Before discussing the implications of the singular behaviour noted above for the eruption region II of figure 1, and the plume III which develops above it, we consider the differences between the axisymmetric flow under discussion and its two-dimensional analogue. Our present calculations suggest that both $\partial u/\partial Y$ and $\partial \theta/\partial Y$, at $Y = 0$, vanish as $x \to \pi$. However the results presented by Merkin (1977), for mixed convection from a circular cylinder, show that in the free-convective limit the corresponding quantities are finite along the upper stagnation line. This shows what one might expect, namely that the boundary layers on each side of the cylinder develop independently and that but for the presence of the other each would penetrate a little way beyond the upper stagnation line before a classical separation was encountered. In the event the two boundary layers impinge upon, or collide with, one another and the flow is forced off into the plume region. In this 'collision' process neither boundary layer anticipates the presence of the other; thus there is no dramatic increase in boundary-layer thickness as the upper stagnation line is approached, and the eruption region in which the flow is re-aligned is on the scale of the thickness of

the oncoming boundary layer. Experimental evidence in favour of this picture of the flow is provided by the flow-visualization pictures of Pera & Gebhart (1972) of such a collision region. These authors conclude from their observations that the usual concept of flow separation is not appropriate in such a situation, but that the impetus for the flow re-alignment is the pressure field generated in the collision region rather than outside the boundary layers. For the problem under consideration in this paper the situation is quite different as the flow converges onto the upper stagnation point, insofar as the boundary layer thickens dramatically, as we have seen, as the eruption region is approached. This feature of such a flow has been observed by Amatò & Tien (1972) and by Jaluria & Gebhart (1975), who again indicate that no flow reversal is present and that the eruption process is more one of flow re-alignment which is independent of any external pressure field. We now return to the consequences of our numerical solution for the flow in the eruption region.

We have noted above that

$$V \sim c_1(\pi - x)^{-2}, \quad \delta \sim c_2(\pi - x)^{-1} \quad \text{as} \quad x \to \pi, \tag{10}$$

and the singular nature of the solution in this limit heralds the failure of the boundary-layer equations as an appropriate set of equations to describe the flow. We may interpret the rapid increase of V in the boundary layer as part of the flow re-alignment process since, as $x \to \pi$, the normal velocity in the boundary layer becomes parallel to the plume axis. On the velocity scale which we have introduced we do not anticipate velocities in excess of $O(1)$. We observe from (10) that $\epsilon^{\frac{1}{4}}V = O(1)$ when $\pi - x = O(\epsilon^{\frac{1}{4}})$, and also that on the scale of the radius of the sphere the boundary-layer thickness is then given by $\epsilon^{\frac{1}{4}}\delta = O(\epsilon^{\frac{1}{4}})$. We have then an eruption region, II of figure 1, of dimensions $\epsilon^{\frac{1}{4}} \times \epsilon^{\frac{1}{4}}$ on the scale of the sphere radius within which velocities are $O(1)$. Introducing these length and velocity scales into the governing equations (1) shows that in the momentum equations we have a balance between the inertia and pressure terms whilst in the energy equation only the convective terms remain. This is consistent with the ideas of Jaluria & Gebhart (1975) discussed above. It may be noted that the collision process associated with two-dimensional flows results in an eruption region which is of much smaller scale. We do not discuss the flow in this eruption region further except to note that both vorticity and temperature will remain constant on the streamlines of the inviscid flow.

It is natural to seek support for the above ideas from the published experimental literature. In the experiments of Kranse & Schenk (1965) solid benzene spheres were melted in excess liquid benzene. The results which are presented for the local Nusselt number show a departure from the monotonic decrease predicted by first-order boundary-layer theory at an angular distance of some 20° to 50° from the upper stagnation point. Jaluria & Gebhart (1975) carry out their experiments with a hemisphere in water, but it seems unlikely that this difference in geometry will affect the flow locally in the neighbourhood of the upper stagnation point. From results presented for the boundary-layer thickness and local heat transfer rate we infer that finite-Grashof-number effects are apparent within 30° of the upper stagnation point. A similar result is obtained from the experiments of Amato & Tien (1972) who work with solid spheres in water. In the experiments described above the Grashof number is in the range 10^6 to 10^8. Now our prediction of an eruption region of dimensions $\epsilon^{\frac{1}{4}} \times \epsilon^{\frac{1}{4}}$ on the scale of the sphere radius (that is $Gr^{-\frac{1}{8}} \times Gr^{-\frac{1}{8}}$) shows that when $Gr = 10^8$

we can expect first-order boundary-theory to fail, and finite-Grashof-number effects to become important, at an angular distance $O(20°)$ from the upper stagnation point. This is consistent with the above observations. Amato & Tien also present temperature and velocity profiles at five different stations which include a horizontal traverse across the upper stagnation point, that is across the eruption region. These profiles show *inter alia* that for $x \leqslant \frac{1}{2}\pi$ the entraining diverging flow thickens only slightly, and the results presented are qualitatively in accord with those shown in figures 2 and 3. However, of greater interest to us here is the traverse across the upper stagnation point. From the temperature profiles, and making due allowance for the tube which supports the sphere, we infer that the thickness of the eruption region is about 8·5 times greater than the thickness of the boundary layer at $x = \frac{1}{2}\pi$. Our theoretical prediction is that it will be thicker by an amount $O(Gr^{\frac{1}{8}})$. Thus for the Grashof numbers in question we would predict that the eruption region is 5·5 to 6·5 times thicker than the boundary layer. We consider that this qualitative agreement between theory and experiment supports our theoretical development for the flow in the neighbourhood of the upper stagnation point.

3. The plume region

The fluid emerges from the eruption region II to form the plume III (see figure 1). It is convenient to retain the same scales for velocity, length and temperature in the plume as we used in § 2. Thus, if x is measured along the plume axis, z measured radially from it, with (u, w) the corresponding components of velocity, we have, from (1),

$$\frac{\partial}{\partial x}(zu) + \frac{\partial}{\partial z}(zu) = 0, \tag{11a}$$

$$u\frac{\partial u}{\partial x} + w\frac{\partial u}{\partial z} = \frac{\epsilon}{z}\frac{\partial z}{\partial}\left(z\frac{\partial u}{\partial z}\right) + \theta, \tag{11b}$$

$$u\frac{\partial \theta}{\partial x} + w\frac{\partial \theta}{\partial z} = \frac{\epsilon}{\sigma z}\frac{\partial}{\partial z}\left(z\frac{\partial \theta}{\partial z}\right), \tag{11c}$$

where, prior to introducing any boundary-layer scaling, we have retained in (11) only the terms from (1) which will ultimately prove to be relevant. Boundary conditions for (11) include, by symmetry,

$$w = \frac{\partial u}{\partial z} = \frac{\partial \theta}{\partial z} = 0 \quad \text{at} \quad z = 0, \tag{12a}$$

and also

$$u, \theta \to 0, \tag{12b}$$

as we move out of the plume.

Before we discuss solutions of (11) note that if we multiply (11*c*) by z and integrate with respect to z then, using (12) and (11*a*), we have

$$\frac{\partial}{\partial x}\int_0^\infty zu\theta\, dz = 0, \tag{13}$$

which shows that the heat flux along the plume is independent of x. This heat flux arises entirely from the heat transferred to the fluid from the surface of the sphere given by (9).

As we have seen in § 2 the fluid emerges from the eruption region to form a plume whose initial diameter is $O(\epsilon^{\frac{1}{2}})$. Thus, at distances $O(1)$ from the sphere, in the plume, we write $z = \epsilon^{\frac{1}{2}}Z$ with $w = \epsilon^{\frac{1}{2}}W$. To first order the equations (11) then become

$$\frac{\partial u}{\partial x} + \frac{1}{Z}\frac{\partial}{\partial Z}(ZW) = 0, \tag{14a}$$

$$u\frac{\partial u}{\partial x} + W\frac{\partial u}{\partial Z} = \theta, \tag{14b}$$

$$u\frac{\partial \theta}{\partial x} + W\frac{\partial \theta}{\partial Z} = 0. \tag{14c}$$

From the last of these we note that if a stream function ψ is introduced such that $u = Z^{-1}\partial\psi/\partial Z$, $W = -Z^{-1}\partial\psi/\partial x$ then $\theta = \theta(\psi)$. The first two equations admit a similarity solution with $\psi = \alpha^2 f(\xi)$, $\xi = Z(x+l_1)^{\frac{1}{4}}/\alpha$, where l_1 corresponds to an origin shift, and α is related to the heat flux in the plume. From (14*b*) we have

$$f'^2 = 2\xi^2\theta,$$

or, since $\theta = \theta(f)$,

$$\sqrt{2}\int_0^\infty \theta^{-\frac{1}{2}}\,df = \xi^2. \tag{15}$$

The solution for f will be determined by (15) when $\theta = \theta(f)$ is known; this will depend upon the details of the solution in the eruption region. (If, as an example, we take $\theta = e^{-2f}$ then $f = \log(1+\xi^2/\sqrt{2})$.) The axial velocity $u = (x+l_1)^{\frac{1}{2}}f'(\xi)/\xi$, and so the constant α will be determined from (13) as

$$\alpha^2\int_0^\infty f'\theta\,d\xi = q, \tag{16}$$

where q is a constant.

In this initial part of the plume region III then, viscous and other diffusive effects are relatively unimportant with the consequence that the axial velocity is eventually $O(x^{\frac{1}{2}})$, the expected 'free-fall' velocity, and the plume thickness is $O\{(\epsilon/x)^{\frac{1}{4}}\}$. This latter result is consistent with the observations of Jaluria & Gebhart (1975) who note that for the plume formed over a hemisphere 'the diameter of the flow region first decreases very rapidly and then begins to increase again'. We shall return to the further development of the plume below, but first we make further comparisons between our results for this initial part of the plume and the experiments of Jaluria & Gebhart, in particular their measurements of centre-line velocity and temperature. To do this we first note that, although the flow in this region is a predominantly inviscid one, there will be a region very close to the axis in which viscous forces are important. Thus if write formally

$$z = \epsilon^{\frac{1}{2}}\bar{Z}, \quad w = \epsilon^{\frac{1}{2}}\bar{W}, \tag{17}$$

with w, x and θ remaining $O(1)$ quantities then all the terms in equations (11) become comparable. For this inner boundary layer conditions as $\bar{Z} \to \infty$ will be provided by the outer inviscid solution. Thus for the velocity u and temperature θ we shall require

$$\left.\begin{aligned} u &\sim (2c)^{\frac{1}{2}}(x+l_1)^{\frac{1}{2}} + O\{\epsilon^{\frac{1}{2}}(x+l_1)\bar{Z}^2\}, \\ \theta &\sim c + O\{\epsilon^{\frac{1}{2}}(x+l_1)^{\frac{1}{2}}\bar{Z}^2\}, \end{aligned}\right\} \tag{18}$$

as $\bar{Z} \to \infty$, where c is a constant. Now the form of the leading terms of (18) suggest a

similarity solution for the boundary-layer equations in this inner region with similarity variable $\tilde{\xi} = \bar{Z}/(x+l_1)^{\frac{1}{4}}$ in terms of which (18) becomes

$$\left.\begin{aligned} u &\sim (2c)^{\frac{1}{2}}(x+l_1)^{\frac{1}{2}} + O\{\epsilon^{\frac{1}{2}}(x+l_1)^{\frac{3}{4}}\tilde{\xi}^2\}, \\ \theta &\sim c + O\{\epsilon^{\frac{1}{2}}(x+l_1)\tilde{\xi}^2\}, \end{aligned}\right\} \tag{19}$$

as $\tilde{\xi} \to \infty$. These conditions suggest in turn that the solution in the inner region be developed as

$$\left.\begin{aligned} \psi &= (x+l_1)\tilde{f}_1(\tilde{\xi}) + \epsilon^{\frac{1}{2}}(x+l_1)^2\tilde{f}_2(\tilde{\xi}) + \ldots, \\ \theta &= \tilde{\theta}_1(\tilde{\xi}) + \epsilon^{\frac{1}{2}}(x+l_1)\tilde{\theta}_2(\tilde{\xi}) + \ldots . \end{aligned}\right\} \tag{20}$$

Substituting (20) into the boundary-layer equations, we deduce immediately that the solution of the equations for $\tilde{f}_1, \tilde{\theta}_1$ which satisfy the conditions (12*a*) and (19) are

$$\tilde{f}_1 = \tfrac{1}{2}(2c)^{\frac{1}{2}}\tilde{\xi}^2, \quad \tilde{\theta}_1 = c; \tag{21}$$

in other words the outer inviscid solution is uniformly valid throughout the plume to this order. The equations satisfied by $\tilde{f}_2$ and $\tilde{\theta}_2$ are coupled linear equations; however we do not pursue these further since the essential information which we require for a comparison with the centre-line measurements of Jaluria & Gebhart (1975) is contained in equations (20) and (21). In commenting upon the centre-line velocities which they present Jaluria & Gebhart note that their results, in which the velocity increases monotonically, are only consistent with the fully developed plume solution (discussed below) in the sense that for each case considered the velocity appears to be approaching a uniform value. In figure 8 we reproduce the experimental results of Jaluria & Gebhart and compare them with curves of the form $(2c)^{\frac{1}{2}}(x+l_1)^{\frac{1}{4}}$, which is the form that we predict for the centre-line velocity in this part of the plume. We are encouraged by the more than qualitative agreement between experiment and the theoretical prediction. However it is when we consider the centre-line temperature that we find a more striking confirmation of our theoretical predictions. From (20*b*) the centre-line temperature is given as $c + \epsilon^{\frac{1}{2}}(x+l_1)\tilde{\theta}_2(0)$, which shows that to leading order we would expect the centre-line temperature to be uniform. In the experiments, where measurements are made to about one diameter above the hemisphere, there is a region of rapid change for about one tenth of a diameter, which is consistent with our estimate of the size of the eruption region, followed by an extensive region of almost uniform temperature. The departure from a constant value is clearly linear to within experimental error, which is exactly the variation of centre-line temperature that we have predicted above. Furthermore the measured slope, for each set of results presented, of the linear temperature variation is $-0{\cdot}011$, which may be compared with the theoretical slope of $O(\epsilon^{\frac{1}{2}}) = O(Gr^{-\frac{1}{4}}) = O(10^{-2})$, for the Grashof numbers associated with the experiments.

Ultimately, as x increases, viscous effects will become important throughout the plume region. To estimate the distance downstream for this state to be established we note that in our inviscid plume solution the axial velocity is $O(x^{\frac{1}{2}})$ and the plume thickness is $O\{(\epsilon/x)^{\frac{1}{4}}\}$. From these two properties of the inviscid plume the viscous term in (11*b*) becomes formally comparable with the other terms when $x = O(\epsilon^{-\frac{1}{2}})$, and that then $u = O(\epsilon^{-\frac{1}{4}})$, $Z = O(\epsilon^{\frac{1}{4}})$ and $W = O(\epsilon^{\frac{3}{4}})$. This estimate of the height at which the plume solution discussed above fails is also recovered from equations (20). Thus in this part of region III, which might be called the classical plume region, we write

$$x = \epsilon^{-\frac{1}{2}}\bar{x}, \quad z = \epsilon^{\frac{3}{4}}\bar{z}, \quad u = \epsilon^{-\frac{1}{4}}\bar{u}, \quad w = \epsilon^{\frac{1}{4}}\bar{w}, \quad \theta = \bar{\theta}, \tag{22}$$

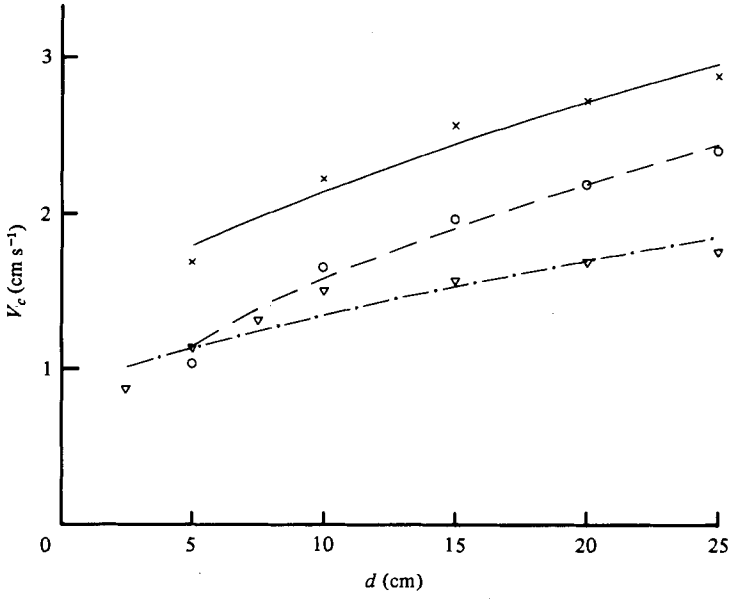

FIGURE 8. A comparison between experimental measurements of the centre-line velocity V_c in the plume formed at distance d immediately above a hemisphere of diameter D due to Jaluria & Gebhart (1975), for various values of the Rayleigh number Ra, with the present theoretical prediction. The experiments were carried out in water with $\sigma = 7{\cdot}0$. Here $Ra = \sigma Gr$ and the Grashof number is based on diameter D. ×, $D = 30{\cdot}5$ cm, $Ra = 6{\cdot}9 \times 10^8$; ——, $V_c = 0{\cdot}53(d + 6{\cdot}55)^{\frac{1}{2}}$. ○, $D = 30{\cdot}5$ cm, $Ra = 20{\cdot}4 \times 10^8$; – – –, $V_c = 0{\cdot}48(d + 0{\cdot}62)^{\frac{1}{2}}$. ▽, $D = 15{\cdot}2$ cm, $Ra = 0{\cdot}86 \times 10^8$; –·–·–·–, $V_c = 0{\cdot}33(d + 7{\cdot}01)^{\frac{1}{2}}$.

and equations (11) then become

$$\left.\begin{aligned} &\frac{\partial}{\partial \bar{x}}(\bar{z}\bar{u}) + \frac{\partial}{\partial \bar{z}}(\bar{z}\bar{w}) = 0, \\ &\bar{u}\frac{\partial \bar{u}}{\partial \bar{x}} + \bar{w}\frac{\partial \bar{u}}{\partial \bar{z}} = \frac{1}{\bar{z}}\frac{\partial}{\partial \bar{z}}\left(\bar{z}\frac{\partial \bar{u}}{\partial \bar{z}}\right) + \bar{\theta}, \\ &\bar{u}\frac{\partial \bar{\theta}}{\partial \bar{x}} + \bar{w}\frac{\partial \bar{\theta}}{\partial \bar{z}} = \frac{1}{\sigma \bar{z}}\frac{\partial}{\partial \bar{z}}\left(\bar{z}\frac{\partial \bar{\theta}}{\partial \bar{z}}\right), \end{aligned}\right\} \tag{23}$$

with boundary conditions

$$\bar{w} = \frac{\partial \bar{u}}{\partial \bar{z}} = \frac{\partial \bar{\theta}}{\partial \bar{z}} = 0, \quad \bar{z} = 0; \quad \bar{u}, \bar{\theta} \to 0 \quad \text{as} \quad \bar{z} \to \infty, \tag{24}$$

together with a heat flux condition derived from (13). A similarity solution of (18), (19), apparently first noted by Prandtl (see Prandtl 1952, p. 413), is available. Thus we have

$$\left.\begin{aligned} \bar{\psi} &= (\bar{x} + l_2) F(\bar{\xi}), \\ \bar{\theta} &= \beta^4 \Theta(\bar{\xi})/(\bar{x} + l_2), \\ \bar{\xi} &= \beta \bar{z}/(\bar{x} + l_2)^{\frac{1}{4}}, \end{aligned}\right\} \tag{25}$$

from which we deduce that $\bar{u} = \beta^2 F'/\bar{\xi}$. In (25) l_2 is a constant associated with an origin shift, and β is a constant related to the heat flux. Thus from (13) and (25)

$$\beta^4 \int_0^\infty F' \Theta \, d\bar{\xi} = q.$$

The solution (25) shows that in the final development of the plume the centre-line velocity is a constant, the temperature falls off inversely with axial distance and the plume grows in thickness as a paraboloid. The nonlinear system of ordinary differential equations for F, Θ has been considered by, for example, Yih (1956) and Fujii (1963) who note exact solutions for specific values of σ, and present numerical solutions for other values.

Jaluria & Gebhart (1975) on the basis of their measurements in the plume, which extend to about one diameter, cautiously suggest that the classical plume state will be reached within three diameters downstream. Our estimate, based upon (22), would suggest a somewhat greater distance although it is unlikely that laminar flow will be maintained up to the point when (25) is achieved.

4. Conclusion

We have analysed the free-convective flow from the surface of a heated sphere at high Grashof number. The boundary-layer solution at the sphere surface has been obtained numerically, and we have demonstrated how the solution fails as the upper stagnation point is approached, and the fluid erupts from the boundary layer to form the plume which develops over the sphere. Initially the plume has thickness $O(a\epsilon^{\frac{1}{4}})$ and within it viscous and other diffusive effects are unimportant. Subsequently, at distances $O(a\epsilon^{-\frac{1}{2}})$ or $O(a\,Gr^{\frac{1}{4}})$ above the sphere, viscous effects do become important and the classical plume solution is recovered. It is only at these distances that the heated sphere may be treated as a point source of heat. Where possible we have compared our work with that of other authors, and in particular we find encouraging agreement between our theoretical predictions and the published experimental results.

Financial support for this work was provided, in part, by a research grant from the Science Research Council.

REFERENCES

Acrivos, A. 1960 *A.I.Ch.E. J.* **6**, 584.

Amato, W. S. & Tien, C. 1972 *Int. J. Heat Mass Transfer* **15**, 327.

Bromham, R. J. & Mayhew, Y. R. 1962 *Int. J. Heat Mass Transfer* **5**, 83.

Chiang, T., Ossin, A. & Tien, C. L. 1964 *Trans. A.S.M.E.* C, *J. Heat Transfer* **86**, 537.

Fujii, T. 1963 *Int. J. Heat Mass Transfer* **6**, 597.

Jaluria, Y. & Gebhart, B. 1975 *Int. J. Heat Mass Transfer* **18**, 415.

Kranse, A. A. & Schenk, J. 1965 *Appl. Sci. Res.* A **15**, 397.

Merk, H. J. & Prins, J. A. 1954 *Appl. Sci. Res.* A **4**, 207.

Merkin, J. 1977 *Int. J. Heat Mass Transfer* **20**, 73.

Pera, L. & Gebhart, B. 1972 *Int. J. Heat Mass Transfer* **15**, 175.

Prandtl, L. 1952 *Essentials of Fluid Dynamics*. Blackie.

Watson, A. & Poots, G. 1972 *Int. J. Heat Mass Transfer* **15**, 1467.

Yih, C.-S. 1956 In *Fluid Models in Geophysics, Proc. 1st Symp. on the Use of Models in Geophysics*. Washington, D.C.: United States Government Printing Office.